Ceramics International 47 (2021) 23045–23052

Contents lists available at ScienceDirect

Ceramics International

journal homepage: www.elsevier.com/locate/ceramint

Effect of graphite and Mn_3O_4 on clay-bonded SiC ceramics for the production of electrically conductive heatable filter

Syed Zaighum Abbas Bukhari [a], Muhammad Shoaib Anwar [a,b], Danyal Naseer [a,b], Jang-Hoon Ha [a], Jongman Lee [a,b], In-Hyuck Song [a,b,*]

[a] Ceramic Materials Division, Korea Institute of Materials Science (KIMS), 797 Changwon-daero, Seongsan-gu, Changwon-si, Gyeongsangnam-do, 51508, South Korea
[b] Department of Advanced Materials Engineering, University of Science and Technology (UST), 217 Gajeong-ro, Yuseong-gu, Daejeon, 34113, South Korea

ARTICLE INFO

Keywords:
SiC
Mullite
Electrical resistivity
Mechanical properties
Manganese oxide

ABSTRACT

Electrically conductive porous SiC ceramics are attracting substantial attention due to their application in heatable filters, vacuum chuck, and semiconductor processing parts, etc. The main problem is their high processing cost. Ideal candidates from an engineering ceramic perspective will be mechanically durable and have the required electrical properties with sufficiently low fabrication costs. To decrease the sintering temperature, kaolin has been added, but it tended to render the material an insulator. Graphite was used to effectively decrease the electrical resistivity. Additionally, manganese oxide was used to decrease the quantity of kaolin (the component that leads to an insulator material after sintering) and decrease the electrical resistivity while maintaining the mechanical properties. In our study, we found that SiC with 35% kaolin, 20% graphite and 10% manganese oxide can produce samples with 6.5×10^{-1} Ω cm electrical resistivity and 43.5 MPa flexural strength at a low sintering temperature of 1200 °C.

1. Introduction

Porous ceramic materials are of substantial interest due to their high performance in solving contemporary issues in the energy, environment, and manufacturing industries. Porous SiC ceramics offer a unique combination of properties such as enhanced chemical, mechanical and thermal stabilities, higher permeability, oxidation and corrosion resistances, and a low coefficient of thermal expansion [1–5]. Due to these superior properties, porous SiC ceramics are widely used in many engineering applications, e.g., in separation membranes [6–8], molten metal filters [9,10], hot-gas filters [11,12], dust collectors [13], catalysis supports [1,14,15], heat exchangers [16,17], thermal insulators [18], and heat sinks [19,20]. For the fabrication of porous SiC-based heatable filters (which are used for contaminated indoor air cleaning), the key parameters to control are the electrical resistivity, thermal conductivity and porosity.

Most of the literature on porous SiC ceramics is based on the processing/control of the pore morphology and the control of mechanical properties. However, interest in the control of electrical properties is increasing [4,21–23]. SiC is categorized as an electrical semiconductor material with wide bandgap energies from 2.4 to 3.3 eV at room temperature that depend on the polytype [24]. The key factors in controlling the electrical conductivity of porous SiC ceramics are the porosity, type of dopant and its concentration, sintering atmosphere and impurities in the raw SiC powders [25–29]. Most of the studies involved two strategies for decreasing the electrical resistivity of dense SiC ceramics: nitrogen doping using nitrogen-containing additives [30–33] and the addition of an electrically conductive carbon-based phase [34–42]. In the literature, it is reported that the addition of a nitrogen-containing liquid phase in the first method causes enhanced grain growth [30], thereby leading to densification. Therefore, this approach is not suitable for the fabrication of porous SiC ceramics. The second strategy involves the addition of carbon nanotubes (CNTs), graphene, graphene oxide and graphite. The electrical resistivity of dense SiC ceramics was decreased via the addition of CNT from 1.1×10^{1} to 2.7×10^{-1} Ω cm [34], via the addition of graphene from 1.0×10^{9} to 5.9×10^{1} Ω cm and from 1.0×10^{0} to 2.3×10^{-1} Ω cm [35–40], via the addition of graphene oxide from 5.8×10^{1}–1.0×10^{0} Ω cm to 4.2×10^{1}–5.5×10^{-1} Ω cm [40,41], and via the addition of graphite from 1.3×10^{2} to 1.0×10^{0} Ω cm [42]. Recently, Kim et al. added graphite to produce porous SiC ceramics with

* Corresponding author. Ceramic Materials Division, Korea Institute of Materials Science (KIMS), 797 Changwon-daero, Seongsan-gu, Changwon-si, Gyeongsangnam-do, 51508, South Korea.
E-mail address: sih1654@kims.re.kr (I.-H. Song).

https://doi.org/10.1016/j.ceramint.2021.05.019
Received 6 March 2021; Received in revised form 26 April 2021; Accepted 3 May 2021
Available online 11 May 2021

Table 1
SiC, kaolin and graphite compositions of the samples.

Sample name	SiC	Kaolin	Graphite	Total
	%	%	%	%
S70K30C0	70	30	0	100
S65K35C0	65	35	0	100
S60K40C0	60	40	0	100
S55K45C0	55	45	0	100
S60K30C10	60	30	10	100
S55K35C10	55	35	10	100
S50K40C10	50	40	10	100
S45K45C10	45	45	10	100
S50K30C20	50	30	20	100
S45K35C20	45	35	20	100
S40K40C20	40	40	20	100
S35K45C20	35	45	20	100

Table 2
Mixture compositions with increasing Mn_3O_4 contents.

Sample name	SiC	Kaolin	Graphite	Mn_3O_4	Total
	%	%	%	%	%
S35K45C20M0	35	45	20	0	100
S35K40C20M5	35	40	20	5	100
S35K35C20M10	35	35	20	10	100
S35K30C20M15	35	30	20	15	100

Table 3
Mixture compositions that contain 50% Mn_3O_4 with 50% SiC (S50M50) and 50% kaolin (K50M50).

Sample name	SiC	Kaolin	Mn_3O_4	Total
	%	%	%	%
S50M50	50		50	100
K50M50		50	50	100

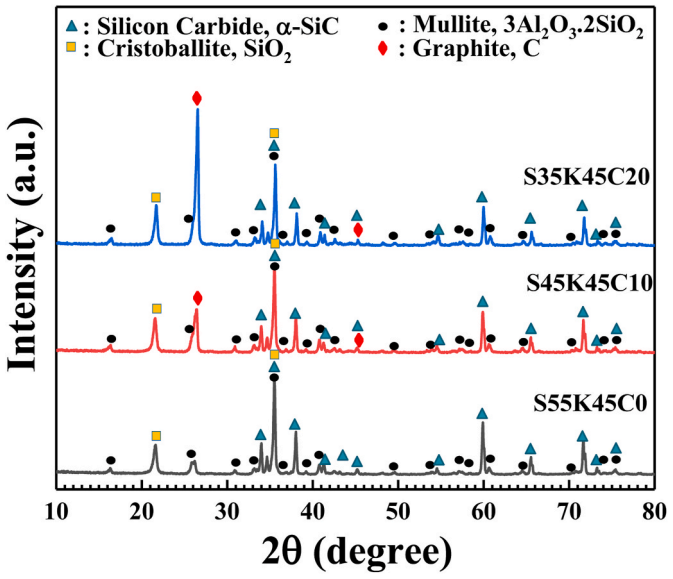

Fig. 1. XRD results of samples that contain mixtures of SiC, kaolin and graphite and were sintered at 1400 °C.

up to 50 wt % graphite content and observed a decrease in electrical resistivity from 3.9×10^{1}–9.0×10^{-2} Ω cm [43]. Thus, graphite was found to effectively decrease the electrical resistivity to produce porous conductive SiC ceramics. All of these studies involve high fabrication costs due to the use of sophisticated techniques and high sintering temperatures (>1800 °C).

Thus, the objective of this study was to propose a composition by which we can realize a low electrical resistivity (up to 10^{-1} Ω cm) with a low sintering temperature while maintaining sufficient mechanical strength. Therefore, in this study, we used a clay-bonded SiC system for low-temperature processing of SiC; however, this system leads to very high electrical resistivity. Graphite was added to the composition to decrease the electrical resistivity since it has very low intrinsic electrical resistivity. Furthermore, manganese oxide (Mn_3O_4) was added for the first time as another inorganic sintering additive besides kaolin, and it was found to form materials with low electrical resistance as a result of phase transformation and reaction with kaolin at higher temperatures [44–46]. The study was divided into two parts: In the first part, the ratio of graphite with respect to clay and SiC for the required electrical properties was optimized. In the second part, the effect of manganese oxide was evaluated for the replacement of kaolin as a sintering additive with enhanced control of electrical properties.

2. Materials and methods

For preparing the pellets, SiC powder (with an average particle size of 4.5 μm) was obtained from Han Song Ltd., China, and kaolin (average particle size 2.1 μm), graphite powder (average particle size 20 μm), and manganese oxide (Mn_3O_4) powder (average particle size ~100 nm) were obtained from Sigma-Aldrich, USA. All powders were mixed by ball milling for 5 h at 200 rpm, with water with a powder to water ratio of 1:2 according to the specified composition in Tables 1–3 in plastic bottles using 10 mm alumina balls (the powder to ball ratio was 1:5) as the mixing medium. After mixing, the balls were separated from the slurry, and the mixture was dried in an oven at 105 °C for 24 h. Then, the mixture was ball milled again for 5 h to convert the dried slurry into powdered form. The resulting powder mixture was uniaxially pressed using a cylindrical die (diameter: 3.6 cm) and a uniaxial load of 20 MPa. After pressing, the samples were sintered at various temperatures with heating and cooling rates of 5 °C/min in an argon gas (99.995%) atmosphere.

XRD patterns for classification of the phases were obtained using an X-ray diffractometer (D/Max-2500VL/PC, Rigaku Co. Ltd., Tokyo, Japan) at 40 kV and 200 mA with a Cu Kα radiation source. The microstructures of the samples were investigated by using low-voltage scanning electron microscopy (LV-SEM, Carl Zeiss, Germany). The linear shrinkage of the pellets was calculated via the following equation:

$$\text{Linear shrinkage } (\%) = \frac{D_g - D_s}{D_g} \times 100 \quad (1)$$

where D_g and D_s are the diameters of the samples of the green sample and sintered sample, respectively. The pore size distribution of the samples was analysed by mercury porosimetry (Autopore IV 9510, Micromeritics, USA). Porosity was determined by the Archimedes method, with distilled water as the liquid medium. To measure the average flexural strength, the mixture pellets were machined into dimensions of 4.0 mm × 4.0 mm × 36 mm, and a four-point bending test (Instron 4206, Instron, USA) was conducted on five samples. The volume electrical resistivity of each sintered sample was evaluated using a MODUSYS 4-point probe analyser (Modusystems, Inc. South Korea).

3. Results and discussion

The study is divided into two parts: First, the effect of graphite is evaluated in SiC and clay systems. Second, the effect of manganese oxide is evaluated.

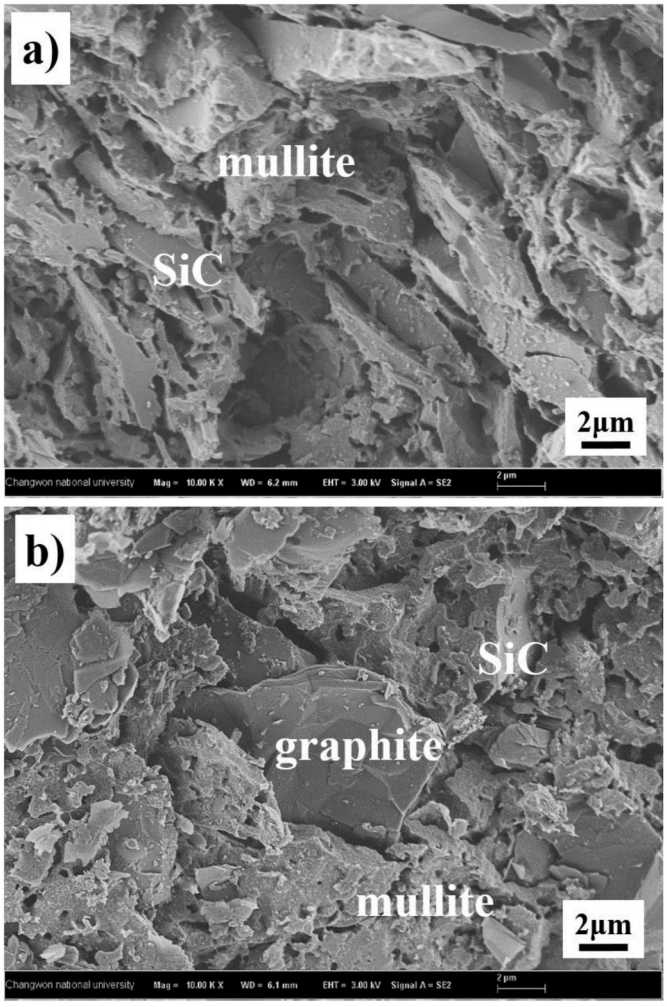

Fig. 2. SEM images of (a) clay-bonded SiC (S55K45C0) and (b) clay-bonded SiC with graphite (S35K45C20), sintered at 1400 °C.

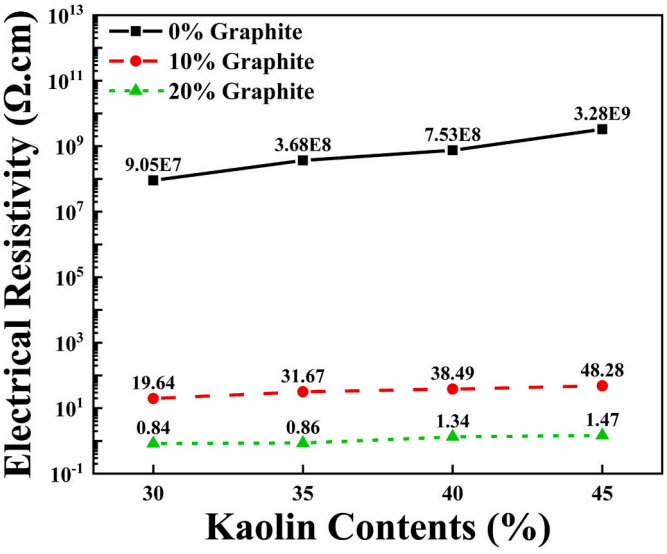

Fig. 3. Effect of the graphite contents and kaolin contents on electrical resistivity of the samples sintered at 1400 °C.

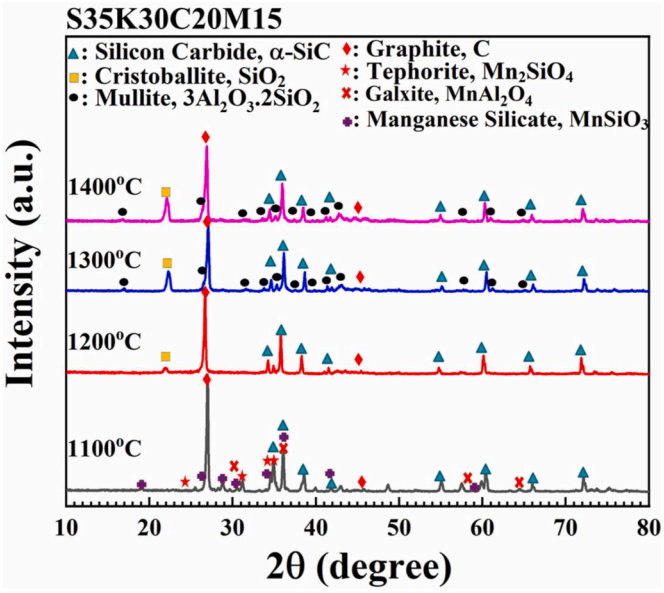

Fig. 4. XRD results that show the effects of sintering temperatures on S35K30C20M15 samples.

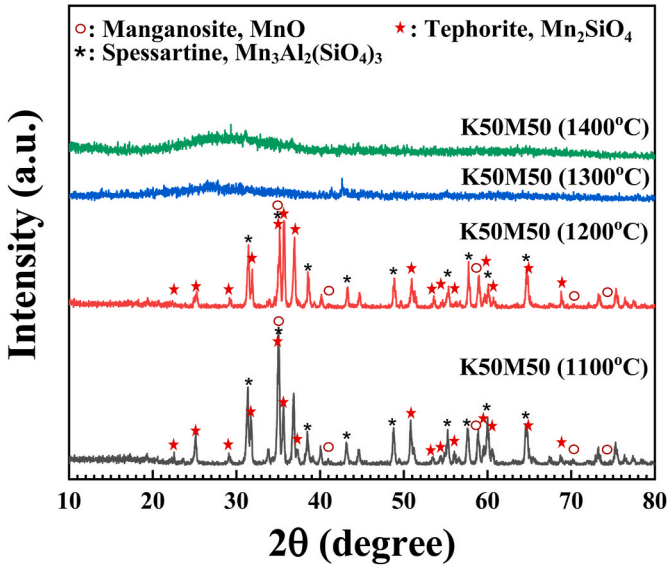

Fig. 5. XRD results that show the effects of the sintering temperature on samples with 50% Mn_3O_4 and 50% kaolin (K50M50).

3.1. *Effect of graphite on clay-bonded SiC*

SiC is a typical engineering ceramic material with a high fabrication cost due to its high sintering temperature. To decrease the sintering temperature, clay was incorporated. Furthermore, graphite was added to control the electrical resistivity of the product. To evaluate the effect of graphite on clay-bonded SiC, samples were prepared according to Table 1 with various concentrations of SiC, kaolin and graphite. In Table 1, each sample is labelled with the first letter of the name of the material, namely, S for SiC, K for kaolin, and C for graphite, and the subsequent number represents the percentage of that material in the composition. This series of the samples will be termed SKC (consisting of SiC, kaolin and graphite) samples.

After preparing the samples according to Table 1, the samples were sintered at 1400 °C for 2 h in an argon atmosphere. XRD of the samples was conducted to evaluate any crystallographic changes after sintering.

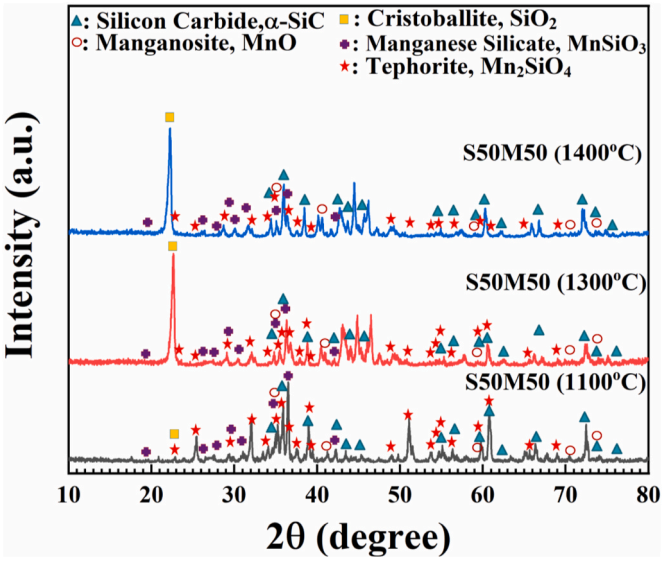

Fig. 6. XRD results that show the effects of the sintering temperature on samples with 50% Mn_3O_4 and 50% SiC (S50M50).

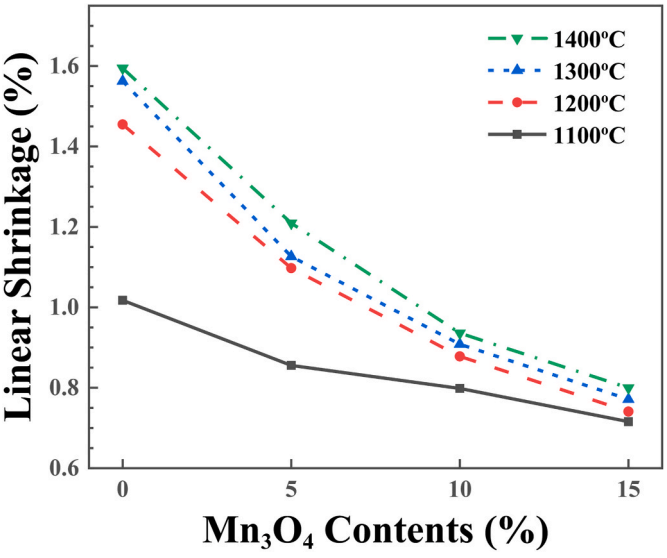

Fig. 7. Effects of the Mn_3O_4 content and sintering temperature on the linear shrinkage of samples.

Fig. 1 shows that the sample that was comprised of only SiC and kaolin had distinctive SiC peaks with mullite and cristobalite. Thus, kaolin was converted into mullite and cristobalite phases, which is a known phase transformation for kaolin [47]. However, no phase transformation for SiC or graphite occurred, and the height of only the graphite peak increased with the addition of graphite. Similarly, according to Fig. 2, when there was only SiC and kaolin, as presented in Fig. 2(a), the SiC particles showed satisfactory connectivity with each other due to the needle-like mullite phase. Whereas in case of S35K45C20, as shown in Fig. 2(b), a large volume of flake like low density graphite powder was incorporated into the clay-bonded SiC samples, the particles were well in contact with each other and become a part of clay and SiC structure.

The objective of adding graphite was to decrease the electrical resistivity of clay-bonded SiC, as graphite is a strong conductor of electricity [48]. Fig. 3 shows the effect of graphite addition into the SiC kaolin system. After sintering at 1400 °C for 2 h in an argon atmosphere, the samples were evaluated in terms of electrical resistivity. Fig. 3 shows

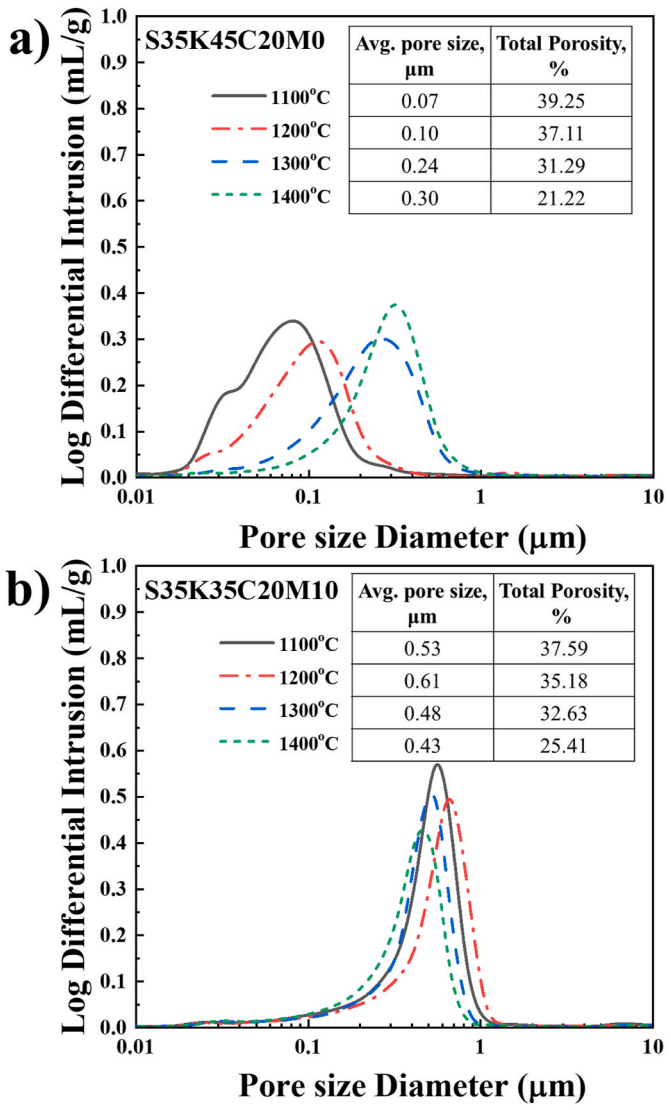

Fig. 8. The effect of the sintering temperature on the pore size distribution and porosity of (a) S35K40C20M0 and (b) S35K35C20M10 samples.

that an increase in kaolin content leads to an increase in electrical resistivity. As shown by Fig. 1, kaolin is converted into mullite and cristobalite, and both materials are electrical insulator materials [49], thus increase in mullite and cristobalite were the reason for increased in electrical resistivity. Whereas an increase in graphite content leads to a logarithmic decrease in electrical resistivity. To further decrease in electrical resistivity more graphite will be required, which could lead to decrease in mechanical strength of the product. Also, decrease in kaolin contents could help to decrease the electrical resistivity. Therefore, it is better to replace kaolin (which causes higher resistivity in the material) with a material that can facilitate sintering at lower temperatures and also help in electrical properties of the material.

3.2. *Effect of manganese oxide on SKC samples*

To increase the flexural strength even at lower temperatures while maintaining the electrical properties, a fourth component, a low melting point additive, manganese oxide (Mn_3O_4) was added to facilitate liquid phase sintering. This section will explain the effect of Mn_3O_4 addition on graphite-containing clay-bonded SiC samples.

Table 2 presents the compositions that were used to prepare the samples. In Table 1, the sintering additive as the binding phase was only

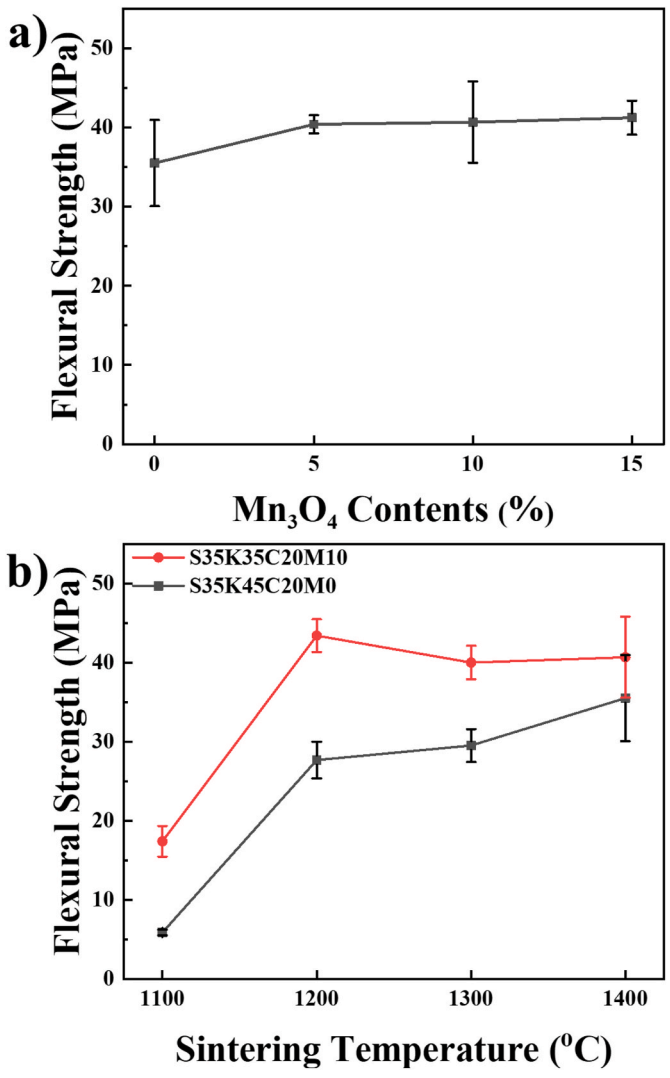

Fig. 9. (a) The effect of the Mn_3O_4 content on the flexural strength of samples that were sintered at 1400 °C and (b) the effect of the sintering temperature on the flexural strength of S35K45C20M0 and S35K35C20M10.

kaolin, whereas, in Table 2, Mn_3O_4 was added, which also acts as a sintering additive similar to a bonding agent [44–46]. The Mn_3O_4 contents were denoted as 'M'. According to Table 2, when we increased the Mn_3O_4 content, we decreased the concentration of kaolin while keeping the concentrations of SiC and graphite constant; hence, the total sintering additive content remained constant at 45% by mass.

To evaluate the changes in the electrical resistivity with increasing sintering temperature and Mn_3O_4 content, changes in the phase composition were evaluated via XRD, shown in Fig. 4. In Fig. 4, the temperature effect on S35K30C20M15 was evaluated. This composition was selected as a reference because it contains maximum Mn_3O_4 (15 wt %) contents. At 1100 °C, in addition to SiC and graphite, kaolin and manganese oxide were identified as manganese silicates and aluminates according to their peaks. At temperatures above 1100 °C, we could not detect the peaks of manganese silicates or aluminates, whereas at 1200 °C, silica from kaolin crystalizes to form cristobalite, and at 1300 °C and above, additionally mullite formation from kaolin was also observed.

In Fig. 4, at 1100 °C, manganese oxide presence was observed as manganese silicates and aluminates and at higher temperatures they were not observed. To explain this phenomenon, manganese oxide phase transformation and its reaction with kaolin will be explained. According to the Dorris et al. [50], when heated to a higher temperature, Mn_3O_4 (tetragonal) is initially converted to Mn_3O_4 (cubic). Then, Mn_3O_4 (cubic) in an inert atmosphere is converted into MnO with the release of oxygen. Thus, at our study temperature, the most common form of manganese oxide was MnO. Therefore, to identify the products of manganese oxide, we can utilize the phase diagram of the MnO–Al_2O_3–SiO_2 system, as reported by Jung et al. [51]. A range of compounds are formed when manganese oxide interacts with silica and alumina; thus, manganese compounds must be present in the samples that contain manganese oxide. From the phase diagram, we observe that in our temperature range, namely, ≤ 1400 °C, the following reactions can occur:

$$3Al_2O_3+3SiO_2 \rightarrow 3Al_2O_3{\cdot}2SiO_2 \text{ (mullite)} + SiO_2 \text{ (cristobalite)}, \quad (2)$$

$$2MnO + SiO_2 \rightarrow Mn_2SiO_4 \text{ (tephorite)} \quad (3)$$

$$MnO + SiO_2 \rightarrow MnSiO_3 \text{ (manganese silicate)} \quad (4)$$

$$2MnO + Al_2O_3 \rightarrow MnAl_2O_4 \text{ (galaxite)} \quad (5)$$

$$3MnO + SiO_2 + Al_2O_3 \rightarrow Mn_3Al_2(SiO_4)_3 \text{ (spessartine)} \quad (6)$$

Further, in order to clarify the effect of the Mn_3O_4 on our material system, new compositions were prepared by adding 50% Mn_3O_4 with 50% SiC and kaolin. The compositions are specified in Table 3.

Fig. 5 presents the effect of the sintering temperature on the phase changes in the samples that were prepared with 50% Mn_3O_4 and 50% kaolin. As shown in Figs. 1 and 4, we expected that we would identify cristobalite and mullite as the products of kaolin at high temperatures, but we instead identified tephorite (Mn_2SiO_4) and spessartine ($Mn_3Al_2(SiO_4)_3$). Thus, from Fig. 5, we can confirm that the components of kaolin, namely, alumina and silica, reacted with manganese oxide and formed compounds with manganese. It was also observed that, until 1200 °C crystallized phases were observed, but after that, we only observe the amorphous phase. Liquefaction of the materials occurs, due to presence of low melting point spessartine (1200 °C). This is also one of the main reasons why the effect of Mn_3O_4 addition in Fig. 4 was not observed.

Similarly, the effects of the sintering temperature on the phase changes in the samples that were prepared with 50% Mn_3O_4 and 50% SiC are shown in Fig. 6. As explained earlier by Dorris et al., at higher temperatures, Mn_3O_4 (cubic) is converted into MnO, and oxygen is released. This oxygen can react with SiC to form silica. This silica can further react with MnO to form tephorite and manganese silicate via equations (3) and (4). According to the XRD results, at 1100 °C, along with SiC peaks, cristobalite, compounds of MnO with silica (i.e., manganese silicate and tephorite) and unreacted MnO phases were present. It was observed that, a very small amount of silica is produced at 1100 °C, which is converted into silicates of manganese, whereas at higher temperatures, all manganese oxides are present as MnO and its relevant silicates, with high concentration of cristobalite. From Figs. 5 and 6, we conclude that Mn_3O_4 reacted with silica from kaolin and SiC oxidation and with alumina from kaolin to form relevant compounds. The concentrations of these compounds are very low; thus, we were unable to detect them based on the XRD results in Fig. 4.

Fig. 7 shows the effect of Mn_3O_4 addition on linear shrinkage with increasing sintering temperature. The temperature variation was examined from 1100 to 1400 °C. According to Fig. 7, with the increase in temperature, for samples without Mn_3O_4 content (i.e., S35K45C20M0), a sharp increase in shrinkage was observed from 1100 to 1200 °C. This increase in shrinkage was attributed to the start of sintering in kaolin-based materials, whereas from 1200 to 1400 °C, an increase in shrinkage was still observed, but the change was very small. This trend corresponds to the further proceeding and completion of the mullitization reaction. On the other hand, the linear shrinkage of the samples decreased with increasing Mn_3O_4 content. There could be two reason for this decrease in linear shrinkage. First, as an increase in the Mn_3O_4 content is accompanied by a decrease in the kaolin content; thus the

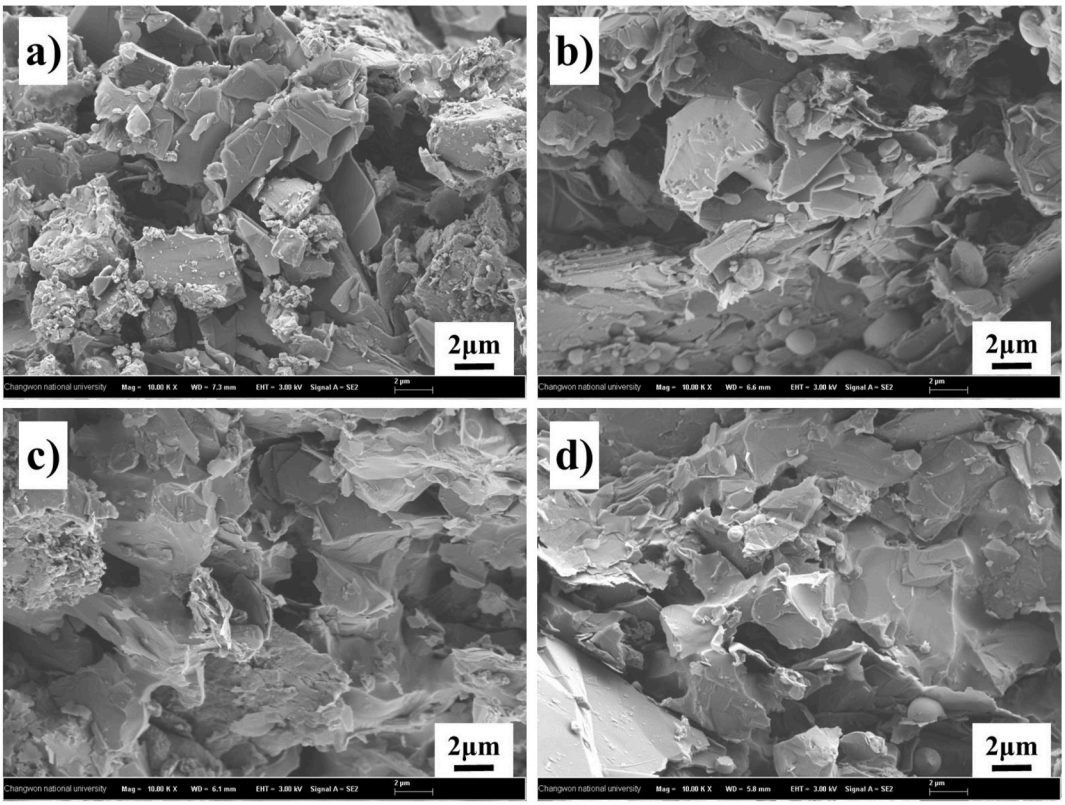

Fig. 10. Effect of the sintering temperature on the microstructures of S35K30C20M15 at (a) 1100 °C, (b) 1200 °C, (c) 1300 °C and (d) 1400 °C.

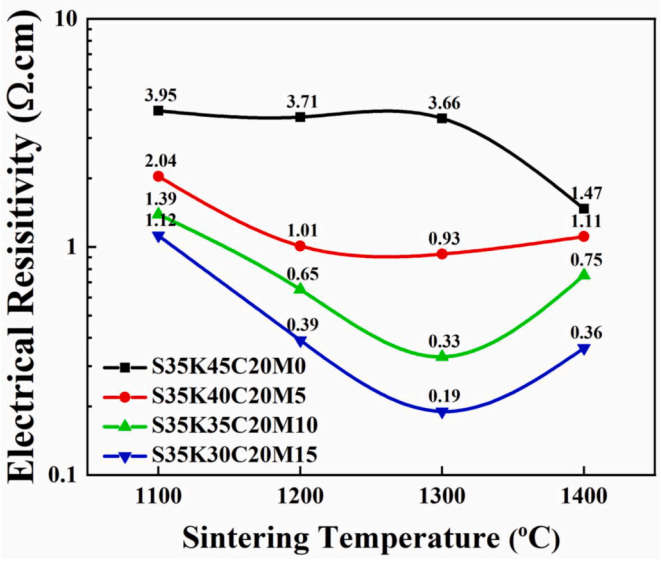

Fig. 11. Effects of the Mn_3O_4 content and sintering temperature on the electrical resistivity of samples.

decrease in shrinkage could be attributed to decrease in kaolin contents or in other terms; kaolin is a more effective additive in the case of an increase in shrinkage. Secondly, as Fig. 6 shows that the reaction of Mn_3O_4 and SiC results in the formation of low-density cristobalite (2.33 g/cm^3) from SiC (3.23 g/cm^3). Thus, the conversion of high-density material with low-density material, cause lesser shrinkage in our samples [52,53]. This kind of behaviour could also affect the pore morphology as well.

Fig. 8(a) and (b) shows the effect of the Mn_3O_4 content and sintering temperature on the porosity and pore size distribution for S35K40C20M0 and S35K35C20M10 samples respectively. From Fig. 8 (a), for S35K45C20M0 samples, we can observe that with the increase in sintering temperature porosity decrease with the increase of pore size [54]. This difference is small in case of 1100 °C and 1200 °C, which may be due to low sinterability of the material at this temperature, but form 1200 °C–1300 °C, a sharp decrease in porosity with increase in average pore size was observed [55]. This may be due to removal of small pores, to become large pores, which is indicative of start of mullitization and sintering in the S35K40C20M0 samples. On the other hand, in Fig. 8(b), for S35K35C20M10 samples, porosity decrease with increasing temperature, but average pore size first shows an increase from 1100 °C to 1200 °C, which is due to high sinterability of S35K35C20M10 samples at this temperature, and then shows a decrease in average pore size with increasing temperature. This decrease in pore size may be caused by combination of two phenomena; conversion of manages silicates into liquid phase, which causes to increase in linear shrinkage, whereas oxidation of SiC leads to increase in low density oxide layer over SiC particles which causes to increased effective particle size [52].

When comparing Fig. 8(a) and (b), we can clearly observe the relatively high average pore size for S35K35C20M10 samples. This could be the result of addition of manganese oxide, which leads to higher sinterability due to reactive sintering and formation of amorphous phase at lower temperature. Due to formation of liquid phase at the particle interface pore coalescence occur during sintering process and higher average pore sizes were observed. It could be appreciated that as heating element, for higher permeability, higher pore size with high porosity is important and the addition of manganese oxide had well contributed in increasing the average pore size.

Fig. 9 shows the effects of the Mn_3O_4 content and sintering temperature on the flexural strength of the samples. Fig. 9(a) shows the effect of increasing Mn_3O_4 content on the flexural strength of samples sintered at 1400 °C. It was observed that at 5 wt %, the flexural strength initially increased slightly and subsequently showed no major change.

Thus, Mn_3O_4 positively impacted the flexural strength of the samples. In addition, we compared the effect of the sintering temperature on S35K45C20M0 samples with that on S35K35C20M10 samples. It was observed that the flexural strength of the S35K45C20M0 sample increased with increasing sintering temperature until 1400 °C. The main bonding phase in this sample was kaolin, which began to convert into mullite and cristobalite at 1200 °C and completed its conversion at approximately 1400 °C [55]. In contrast, the S35K35C20M10 sample shows an initial sharp increase in flexural strength from 1100 to 1200 °C, which is similar to the trend of the S35K45C20M0 sample, but the flexural strength was comparably higher, and from 1200 to 1400 °C, a negative slope in trend was observed. At 1200 °C, reaction sintering occurred due to the reaction of Mn_3O_4 with kaolin and SiC; thus, the maximum flexural strength was attained. According to Fig. 5, at temperatures below 1300 °C, crystalline phases that were formed by the reaction of kaolin and manganese oxide were converted into an amorphous state at 1300 °C; thus, due to the formation of an amorphous phase, the strength was decreased.

Fig. 10 shows the fracture microstructure of S35K30C20M15 samples that were sintered at various temperatures. The sinterability increased with the sintering temperature. At 1100 °C, the samples were not well sintered, as a mullitization reaction was not initiated [55–57]. At 1200 °C, as shown in Fig. 10, particle-to-particle necking was well established, which is indicative of increased volume shrinkage and, thus, increased mechanical strength. Above 1300 °C, the microstructure did not show substantial changes; we can relate this phenomenon with the mechanical strength of the samples at 1300 °C, and above 1300 °C, the mechanical strength did not change substantially.

The electrical resistivity results of the samples are presented in Fig. 11. For the S35K45C20M0 samples, which don't contain Mn_3O_4, the electrical resistivity shows no change until 1300 °C, whereas at 1400 °C, a decreasing trend is observed, which may be associated with increased densification in the samples. For samples other than S35K45C20M0, an initial decrease in electrical resistivity from 1100 to 1300 °C and a subsequent increase in electrical resistivity from 1300 to 1400 °C, with a minimum value at 1300 °C, was observed. The first decrease in electrical resistivity from 1100 to 1300 °C may be due to combination of two things; first decrease in kaolin content and the other due to formation of low electrical resistivity materials by the reaction of manganese oxide with kaolin and SiC, and the increase in electrical resistivity from 1300 to 1400 °C may be due to the conversion of these low electrical resistivity materials into the liquid phase and relatively higher rate of formation of high resistivity cristobalite and mullite. We have also observed that the slopes of the S35K40C20M5 to S35K30C20M15 samples from 1100 to 1300 °C increased with respect to the added Mn_3O_4 contents, which is indicative of the role of Mn_3O_4 in decreasing the electrical resistivity of the samples.

4. Conclusions

In this study, we examined the effects of graphite and Mn_3O_4 on clay-bonded SiC ceramics for the production of electrically conductive heatable filters. It was observed that kaolin has a role of producing SiC-based ceramics at low temperature, but it led to high electrical resistance of the product. Graphite was identified as a better option that could effectively decrease the volume resistivity from 3.28×10^9 to 1.86×10^1 Ω cm; however, graphite addition was associated with a decrease in the mechanical strength. Mn_3O_4 was found to be a highly satisfactory sintering additive that outperformed kaolin in terms of decrease in electrical resistivity and promoted liquid phase sintering, thereby leading to increased mechanical strength, with controlled electrical resistance. When considering the average pore size, porosity, flexural strength and electrical resistivity as low temperature as 1200 °C, sample S35K35C20M10 exhibited gives the optimum results, i.e., an average pore size 0.61 μm with 35.18% porosity, a flexural strength of 43.5 MPa and an electrical resistivity of 6.5×10^{-1} Ω cm.

Declaration of competing interest

The authors declare that they have no known competing financial interests or personal relationships that could have appeared to influence the work reported in this paper.

Acknowledgements

This work was supported by (1) National R&D Program through the National Research Foundation of Korea (NRF) funded by Ministry of Science and ICT [grant number 2020M3H4A3106359] and (2) the Research Program of the Korea Institute of Materials Science (Republic of Korea) [grant number PNK 7420].

References

[1] M.J. Ledoux, S. Hantzer, C. Pham-Huu, J. Guille, M.P. Desaneaux, New synthesis and uses of high-specific-surface SiC as a catalytic support that is chemically inert and has high thermal resistance, J. Catal. 114 (1988) 176–185.
[2] V. Suwanmethanond, E. Goo, P.K.T. Liu, G. Johnston, M. Sahimi, T.T. Tsotsis, Porous silicon carbide sintered substrates for high-temperature membranes, Ind. Eng. Chem. Res. 39 (2000) 3264–3271.
[3] C. Soto, C. Garcia-Rosales, J. Echeberria, J.M. Martinez-Esnaola, T. Hernandez, M. Malo, E. Platacis, F. Muktepavela, SiC-based sandwich material for flow channel inserts in DCLL blankets: manufacturing, characterization, corrosion tests, Fusion Eng. Des. 124 (2017) 958–963.
[4] S. Kultayeva, J.H. Ha, R. Malik, Y.W. Kim, K.J. Kim, Effects of porosity on electrical and thermal conductivities of porous SiC ceramics, J. Eur. Ceram. Soc. 40 (2020) 996–1004.
[5] C. Soto, C. García-Rosales, J. Echeberria, E. Platacis, A. Shisko, F. Muktepavela, M. Malo, T. Hernández, Characterization and thermomechanical assessment of a SiC-sandwich material for flow channel inserts in DCLL blankets, Fusion Eng. Des. 146 (2019) 1983–1987.
[6] M. Fukushima, Y. Zhou, Y.I. Yoshizawa, Fabrication and microstructural characterization of porous silicon carbide with nano-sized powders, Mater. Sci. Eng. B 148 (2008) 211–214.
[7] Y. Zhou, M. Fukushima, H. Miyazaki, Y. Yoshizawa, K. Hirao, Y. Iwamoto, K. Sato, Preparation and characterization of tubular porous silicon carbide membrane supports, J. Membr. Sci. 369 (2011) 112–118.
[8] F. Chen, X. Huang, Y. Wang, Y. Zhang, Z. Hu, Investigation on foam ceramic filter to remove inclusions in revert superalloy, Mater. Lett. 34 (1998) 372–376.
[9] J.H. Eom, Y.W. Kim, S. Raju, Processing and properties of macroporous silicon carbide ceramics: a review, J. Asian Ceram. Soc. 1 (2013) 220–242.
[10] R. Pachaiyappan, R. Gopinath, S. Gopalakannan, Processing techniques of a silicon carbide heat exchanger and its capable properties-a review, Appl. Mech. Mater. 787 (2015) 513–517.
[11] S.C. Kim, Y.W. Kim, I.H. Song, Processing and properties of glass-bonded silicon carbide membrane supports, J. Eur. Ceram. Soc. 37 (2017) 1225–1232.
[12] D. Das, S. Baitalik, B. Haldar, R. Saha, N. Kayal, Preparation and characterization of macroporous SiC ceramic membrane for treatment of waste water, J. Porous Mater. 25 (2018) 1183–1193.
[13] P. Wan, J. Wang, Highly porous nano-SiC with very low thermal conductivity and excellent high temperature behavior, J. Eur. Ceram. Soc. 38 (2018) 463–467.
[14] P. Wan, Z. Wu, H. Zhang, L.Y. Gao, J.Y. Wang, Porous nano-SiC as thermal insulator: wisdom on balancing thermal stability, high strength and low thermal conductivity, Mater. Res. Lett. 4 (2016) 104–111.
[15] C. Liang, Z. Wang, L. Wu, X. Zhang, H. Wang, Z. Wang, Light and strong hierarchical porous SiC foam for efficient electromagnetic interference shielding and thermal insulation at elevated temperatures, ACS Appl. Mater. Interfaces 9 (2017) 29950–29957.
[16] H. Liu, C.Y. Li, X.Y. Ren, K.Q. Liu, J. Yang, Fine platinum nanoparticles supported on a porous ceramic membrane as efficient catalysts for the removal of benzene, Sci. Rep. 7 (2017).
[17] M. Fuji, Y. Shiroki, R.L. Menchavez, H. Takegami, M.Takahashi H. Suzuki, S. Izuhara, T. Yokoyama, Fabrication of cordierite filters by in-situ solidification for high temperature dust collection, Powder Technol. 172 (2007) 57–62.
[18] Z. Zhang, Z. Shi, B. Yang, B. Ge, X. Zhang, Y. Guo, Preparation and anisotropic thermo-physical properties of SiC honeycomb/Al-Mg-Si composite via spontaneous infiltration, Prog. Nat. Sci.: Met. Mater. Int. 29 (2019) 177–183.
[19] J. Li, H. Lin, J. Li, Factors that influence the flexural strength of SiC-based porous ceramics used for hot gas filter support, J. Eur. Ceram. Soc. 31 (2011) 825–831.
[20] A. Dey, N. Kayal, O. Chakrabarti, Permeability and nanoparticle filtration assessment of cordierite-bonded porous SiC ceramics, Ind. Eng. Chem. Res. 52 (2013) 18362–18372.
[21] J. Ihle, H.P. Martin, M. Hermann, P. Obenaus, J. Adler, W. Hermel, A. Michaelis, The influence of porosity on the electrical properties of liquid-phase sintered silicon carbide, Int. J. Mater. Res. 97 (2006) 649–656.
[22] Y. Taki, M. Kitiwan, H. Katsui, T. Goto, Electrical and thermal properties of nitrogen-doped SiC sintered body, J. Jpn. Soc. Powder Powder Metall. 65 (2018) 508–512.

[23] C. Soto, C. García-Rosales, J. Echeberria, E. Platacis, A. Shisko, F. Muktepavela, T. Hernández, M.M. Huertac, Development, characterization, and testing of a SiC-based material for flow channel inserts in high-temperature DCLL blankets, IEEE Trans. Plasma Sci. IEEE Nucl. Plasma Sci. Soc. 46 (2018) 1561–1569.
[24] H.P. Iwata, U. Lindefelt, S. Oberg, P.R. Briddon, Stacking faults in silicon carbide, Physica B 340–342 (2003) 165–170.
[25] K.J. Kim, K.M. Kim, Y.W. Kim, Highly conductive SiC ceramics containing Ti2CN, J. Eur. Ceram. Soc. 34 (2014) 1149–1154.
[26] K.J. Kim, Y.W. Kim, K.Y. Lim, T. Nishimura, E. Narimatsu, Electrical and thermal properties of SiC-AlN ceramics without sintering additives, J. Eur. Ceram. Soc. 35 (2015) 2715–2721.
[27] Y.K. Seo, Y.W. Kim, K.J. Kim, W.S. Seo, Electrically conductive SiC-BN composites, J. Eur. Ceram. Soc. 36 (2016) 3879–3887.
[28] Y.W. Kim, Y.H. Kim, K.J. Kim, Electrical properties of liquid-phase sintered silicon carbide ceramics: a review, Crit. Rev. Solid State 45 (2020) 66–84.
[29] Y.W. Kim, E. Tochigi, J. Tatami, Y.H. Kim, S.H. Jang, S. Javvaji, J. Jung, K.J. Kim, Y. Ikuhara, Carrier depletion near the grain boundary of a SiC bicrystal, Sci. Rep. 9 (2019) 18014.
[30] Y.W. Kim, T.Y. Cho, K.J. Kim, Effect of grain growth on electrical properties of silicon carbide ceramics sintered with gadolinia and yttria, J. Eur. Ceram. Soc. 35 (2015) 4137–4142.
[31] S.H. Jang, Y.W. Kim, K.J. Kim, Effects of Y2O3-RE2O3 (RE = Sm, Gd, Lu) additives on electrical and mechanical properties of SiC ceramics containing Ti2CN, J. Eur. Ceram. Soc. 36 (2016) 2997–3003.
[32] Y.H. Kim, Y.W. Kim, K.J. Kim, Electrically conductive SiC ceramics processed by pressureless sintering, Int. J. Appl. Ceram. Technol. 16 (2019) 843–849.
[33] Y.W. Kim, Y.H. Kim, K.J. Kim, Electrical properties of liquid-phase sintered silicon carbide ceramics: a review, Crit. Rev. Solid State 45 (2020) 66–84.
[34] E.T. Thostenson, P.G. Karandikar, T.W. Chou, Fabrication and characterization of reaction bonded silicon carbide/carbon nanotube composites, J. Phys. D Appl. Phys. 38 (2005) 3962–3965.
[35] L.S. Walker, V.R. Marotto, M.A. Rafiee, N. Koratkar, E.L. Corral, Toughening in graphene ceramic composites, ACS Nano 5 (2011) 3182–3190.
[36] P. Miranzo, C. Ramirez, B. Roman-Manso, L. Garzon, H.R. Gutierrez, M. Terrones, C. Ocal, M.I. Osendi, M. Belmonte, In situ processing of electrically conducting graphene/SiC nanocomposites, J. Eur. Ceram. Soc. 33 (2013) 1665–1674.
[37] B. Roman-Manso, E. Domingues, F.M. Figueiredo, M. Belmonte, P. Miranzo, Enhanced electrical conductivity of silicon carbide ceramics by addition of graphene nanoplatelets, J. Eur. Ceram. Soc. 35 (2015) 2723–2731.
[38] B. Roman-Manso, F.M. Figueiredo, B. Achiaga, R. Barea, D. Perez-Coll, A. Morelos-Gomez, M. Terrones, M.I. Osendi, M. Belmonte, P. Miranzo, Electrically functional 3D-architectured graphene/SiC composites, Carbon 100 (2016) 318–328.
[39] K. Markandan, J.K. Chin, M.T.T. Tan, Recent progress in graphene based ceramic composites: a review, J. Mater. Res. 32 (2017) 84–106.
[40] O. Hanzel, Z. Lences, Y.W. Kim, J. Fedor, P. Saigalik, Highly electrically and thermally conductive silicon carbide-graphene composites with yttria and scandia additives, J. Eur. Ceram. Soc. 40 (2020) 241–250.
[41] O. Hanzel, R. Sedlak, J. Sedlacek, V. Bizovska, R. Bystricky, V. Girman, A. Kovalcikova, J. Dusza, P. Saigalik, Anisotropy of functional properties of SiC composites with GNPs, GO and in-situ formed graphene, J. Eur. Ceram. Soc. 37 (2017) 3731–3739.
[42] Y. Taki, M. Kitiwan, H. Katsui, T. Goto, Electrical and thermal properties of off-stoichiometric SiC prepared by spark plasma sintering, J. Asian Ceram. Soc. 6 (2018) 95–101.
[43] G.D. Kim, Y.W. Kim, I.H. Song, K.J. Kim, Effects of carbon and silicon on electrical, thermal, and mechanical properties of porous silicon carbide ceramics, Ceram. Int. 46 (2020) 15594–15603.
[44] K. Jin-Ho, B. Seung-Woo, Sintering and optical properties of Al_2O_3 ceramics with Mn_3O_4 added, J. Kor. Inst. Elect. and Electron. Mat. Engrs. 29 (2016) 539–545.
[45] B.S.B. Karunaratne, Differing effects of Mn and Mg oxide sintering aids on sialon creep and fracture, J. Mater. Synth. Process. 6 (1998) 433–439.
[46] Z. Hongming, L. Jian, Y. Danqing, X. Lairong, Effect of manganese oxide on the sintered properties of 8YSZ, Phys. Proc. 22 (2011) 14–19.
[47] F.J.M.R. de, S.J.R. Sousa, N.G.d. Araújo, F.H. Carlos, S.L.N.d. Lima, Influence of processing variables on clay-based ceramic formulations, Mat. Res. 22 (2019) 1–9.
[48] Z. Wenge, W. Shing-Chung, Electrical conductivity and dielectric properties of PMMA/expanded graphite composites, Compos. Sci. Technol. 63 (2003) 225–235.
[49] N.S. Mehta, P.K. Sahu, P. Tripathi, R. Pyare, M.R. Majhi, Influence of alumina and silica addition on the physico-mechanical and dielectric behavior of ceramic porcelain insulator at high sintering temperature, Bol. Soc. Espanola Ceram. Vidr. 57 (2018) 151–159.
[50] S.E. Dorris, T.O. Mason, Electrical properties and cation valencies in Mn_3O_4, J. Am. Ceram. Soc. 71 (1988) 379–385.
[51] I.H. Jung, Y. Kang, S.A. Decterov, Thermodynamic evaluation and optimization of the MnO-Al_2O_3 and MnO-Al_2O_3-SiO_2 systems and applications to inclusion engineering, Metall. Mater. Trans. B 35 (2004) 259–268.
[52] S.Z.A. Bukhari, J.-H. Ha, J. Lee, I.-H. Song, Oxidation-bonded SiC membrane for microfiltration, J. Eur. Ceram. Soc. 38 (2018) 1711–1719.
[53] S.Z.A. Bukhari, J.-H. Ha, J. Lee, I.-H. Song, Effect of different heat treatments on oxidation-bonded SiC membrane for water filtration, Ceram. Int. 44 (2018) 14251–14257.
[54] J. Kim, J.-H. Ha, J. Lee, I.-H. Song, The effect of MnO_2 content on the permeability and electrical resistance of porous alumina-based ceramics, J. Kor. Ceram. Soc. 54 (2017) 331–339.
[55] C.Y. Chen, G.S. Lan, W.H. Tuan, Microstructural evolution of mullite during the sintering of kaolin powder compacts, Ceram. Int. 26 (2000) 715–720.
[56] P. Ptáček, M. Křečková, F. Šoukal, T. Opravil, J. Havlica, J. Brandštetr, The kinetics and mechanism of kaolin powder sintering I. The dilatometric CRH study of sinter-crystallization of mullite and cristobalite, Powder Technol. 232 (2012) 24–30.
[57] S. Lee, J.-H. Ha, J. Lee, I.-H. Song, Enhanced mechanical strength of talc-containing porous kaolin prepared by a replica method, J. Kor. Ceram. Soc. 58 (2021) 123–133.